H2 anisotropic subdiffusion and induced expansion in portlandite, gibbsite, and boehmite

Tulio Honorio, Marwane Trifa, Thibaut Herin, Sophie Le Caër

H_2 anisotropic subdiffusion and induced expansion in portlandite, gibbsite and boehmite

Tulio Honorio,*,†,§ Marwane Trifa,† Thibaut Herin,‡,¶ and Sophie Le Caer¶

†*Université Paris-Saclay, CentraleSupélec, ENS Paris-Saclay, CNRS, LMPS - Laboratoire de Mécanique Paris-Saclay, 91190, Gif-sur-Yvette, France.*

‡*Université Paris-Saclay, CEA, Service de recherche en Corrosion et Comportement des Matériaux, 91191, Gif-sur-Yvette, France*

¶*Université Paris-Saclay, CEA, CNRS, NIMBE UMR 3685, 91191 Gif-sur-Yvette, France*

§*Current address: Université Paris-Saclay, CEA, Service de recherche en Corrosion et Comportement des Matériaux, 91191, Gif-sur-Yvette, France*

E-mail: tulio.honoriodefaria@cea.fr

Phone: +33(0)1 69 08 14 47

Abstract

(Oxy)hydroxides such as portlandite ($Ca(OH)_2$), boehmite (γ-AlOOH), and gibbsite (γ-$Al(OH)_3$) have been shown to produce and store dihydrogen or its precursor, the $H^{\cdot}$ atom when subjected to ionizing radiation. In this study, we investigate the diffusion of H_2 and the associated lattice expansion within these three minerals using molecular simulations. The crystal structure of all three (oxy)hydroxides dilates linearly with the number of H_2 molecules introduced, up to approximately 0.5 H_2 per nm^3. The energy barriers between hopping sites are compared with available data from quantum simulations for boehmite and gibbsite, and are provided for the first time for portlandite. H_2 diffusion in these materials is shown to be subdiffusive, which might

explain why such systems have to be activated, for example, by heating, to release the H_2 molecules. Nevertheless, simulations also show that each system has its own specific behavior related to anisotropy in diffusion: H_2 is effectively trapped in gibbsite, shows 1D diffusion in boehmite, and 2D diffusion in portlandite. H_2 migration can be observed under experimentally attainable timescales in defect-free boehmite and portlandite, but not in gibbsite below 100°C. The affinity of H_2 with the bulk mineral (quantified using a damping factor multiplied to the potential well energy of the H_2 force field) together with the considerations about the connectivity of interstitial sites explains the subdiffusive behavior in the minerals studied.

Introduction

In cemented nuclear waste packages, the potential accumulation of H_2 is a risk that needs to be assessed. This is why numerous studies have focused on the H_2 radiolytic yield measurement and the reaction mechanisms accounting for this production.[1–5] However, in some specific cases, in addition to immediate production, it has been shown that H_2 or its precursors can also remain trapped within the material.[3,5] This was the case for boehmite (γ-AlOOH), gibbsite (γ-$Al(OH)_3$), and portlandite ($Ca(OH)_2$), which raises questions about the specific nature of these materials in terms of H_2 diffusion.

Boehmite and (dry) gibbsite are found in aluminum-clad nuclear fuel in reactors and nuclear waste disposal. Portlandite is one of the major products of ordinary cement hydration, being therefore found in cemented nuclear wastes. These three minerals have similar layered structures but exhibit distinct H_2 radiolytic yields. Temperature dependence of H_2 release was reported for boehmite, and diffusion-driven mechanism including the recombination of $H^{\cdot}$ in the bulk was suggested.[4] Typical H_2 radiolytic yields of portlandite, including delayed H_2 production recently reported,[5] are on the order of 10^{-8} mol/J while boehmite's is on the order of 10^{-9} mol/J.[3] The release of H_2 trapped in (oxy)hydroxides might be associated with solid diffusion through the bulk crystalline structure.[3,5] Understanding H_2 migration in

(oxy)hydroxides is crucial for evaluating the security of nuclear waste disposal.[6] Discussion based on quantum calculations suggests that diffusion plays a critical role in the higher H_2 yields measured for boehmite in comparison with gibbsite.[6]

Previous ^1H NMR experiments have demonstrated the presence of H_2 trapped within portlandite.[5] In this work, a quantitative analysis of the NMR signal of trapped H_2 was performed as a function of time and temperature, and this was coupled with micro-chromatography experiments measuring the H_2 released into the atmosphere. Trapped H_2 within the material was unequivocally identified, and it was shown that it can slowly diffuse to the surface and be released into the atmosphere. In the case of portlandite, although the dimerization of hydrogen atoms within the material is an attractive possibility for accounting for H_2 production, another possibility is that hydrogen atoms react with CaOH groups within the material, forming $CaO^{\bullet}$ radicals and dihydrogen molecules. Although this latter reaction has a lower rate constant than that of the recombination of two hydrogen atoms, the large number of CaOH groups present suggests that the second reaction route is the most probable.

Dihydrogen diffusion in crystalline materials generally occurs via the hopping of hydrogen atoms through the preferential interstitial sites in the crystal lattice.[6] Under real applications, the influence of defects in the lattice (including vacancies, phase, and grain boundaries),[7] and crystal dilation due to temperature rise (associated with certain irradiation conditions) might affect H_2 transport. The mechanisms of diffusion of H_2 in portlandite remain poorly explored. The introduction of H_2 in the crystal lattice is associated with crystal dilatation, as already observed for portlandite irradiated using the 2.5 MeV SIRIUS electron accelerator.[8] In critical cases, hydrogen presence will induce damage.[9] Quantifying the contribution of the effects of temperature, H_2-induced dilatation, and crystal defects in diffusion is essential to understanding dihydrogen migration in (oxy)hydroxides.

Classical molecular dynamics (MD) simulations enable assessing larger times and length scales required to characterize diffusion and H_2-induced dilatation compared to quantum calculations. Simulations up to the nanosecond have been deployed to capture the diffusive

behavior of H_2.[7,10] Fully exploring the effects of H_2-induced dilatation requires simulating a certain number of unit cells. Since H_2 diffusion in crystals occurs mainly via the hopping through the interstitial sites, the energy barrier obtained following the minimum energy path between two hopping sites informs on the diffusion propensity.[6] Since H_2 is quite a small molecule, its dynamics might be potentially subjected to significant quantum effects. Verifying the ability of empirical force fields for (oxy)hydroxides and H_2 to capture these energy barriers will build confidence in using classical MD to simulate H_2 in (oxy)hydroxides.

This study quantifies H_2 diffusion in boehmite, gibbsite, and portlandite using classical molecular simulations. Firstly, we verify the compatibility of ClayFF (one of the most used empirical force fields to model (oxy)hydroxides) with empirical force fields used to model H_2 by comparing the energy barrier associated with hopping sites with results of DFT simulations for boehmite and gibbsite from the literature.[6] Then, we quantify the diffusion in the crystals by assessing the mean-squared displacement H_2 in a dilute system up to 275°C, i.e., a temperature below dehydration of the minerals studied. Anisotropy in diffusion and deviations from normal (Fickean) diffusive regimes are quantified and discussed. The H_2-induced dilatation coupled with temperature increase is evaluated for all the crystals. Collective effects in diffusion are assessed. Finally, we propose a discussion on the nature of the subdiffusive behavior observed.

Materials and methods

Atomic structures and force fields

The structures of boehmite ($Cmc2_1$ space group) resolved by Christensen et al.,[11] gibbsite ($P2_1/n$ space group) resolved by Saalfeld et al.,[12] and portlandite ($P\bar{3}m1$ space group) by Henderson et al.[13] (25°C) were used. Simulation boxes were obtained after replicating the unit cell so that each dimension had at least 2 nm (i.e., twice the cutoff used for short-range interactions). For boehmite, it is a 7x2x6 unit cell; for gibbsite, 3x4x2 unit cell; 6x6x6 for

portlandite. Cartesian and crystallographic frames are indicated in the Figure 1 (details on the unit cells are shown in Fig. S1 in the Supporting Information). Note that in gibbsite and portlandite the c vector is perpendicular to the Al and Ca planes, respectively, whereas in boehmite b vector is perpendicular to the Al plane. Cartesian frames are defined as indicated in the same figure.

ClayFF,[14,15] a force field originally developed to model (oxy)hydroxides like clay minerals, portlandite, and boehmite and their various physical properties (including elasticity, diffusion, thermal and interfacial properties) was adopted to model these three minerals. ClayFF yields lattice parameters consistent with experimental data at ambient temperature (as shown in Table S1 of the Supporting Information)

One- and two-site force fields were used to model H_2, those developed by Köster et al.,[16] Buch,[17] Hirschefelder et al.[18] (one site), and Cracknell[19] (two sites). All these force fields use only the Lennard-Jones potential for intermolecular interactions with hydrogen. The parameters are recalled in the Supporting Information. Lorentz-Berthelot combining rules were applied to mix the Lennard-Jones potentials. These H_2 force fields have been deployed together with force fields for various other crystalline and microporous phases. Buch[17] potential was used to study H_2 diffusion and adsorption in metal-organic and covalent-organic frameworks,[20,21] zeolites,[21] carbon nanotubes,[22] and graphene.[23] Cracknell[19] was originally deployed to study adsorption into graphitic nanofibers. Hirschfelder et al.[18] was combined with ClayFF to study H_2 diffusion in montmorillonite.[10] Köster et al.[16] is the most recent of these force fields and has been developed to improve the description of thermodynamic data of H_2 in fluid mixtures. Since only non-reactive force fields are used, the possibility of dissociation or interactions involving charge transfer with the (oxy-)hydroxides cannot be accounted for. For the one-site force fields, dissociation cannot be contemplated. This aspect has consequences for the definition of lattice diffusion, with the entropy of activation therefore remaining constant for the processes considered.

Simulation details

Simulations were run with LAMMPS[24] with periodic boundary conditions. Tail corrections were added to Lennard-Jones potentials. The cutoff for short-range interaction was 10 Å. Particle-particle particle-mesh solver was used to cope with long-range electrostatics.

Energy barriers

Since H_2 diffusion in crystals occurs mainly via the hopping through the interstitial sites, the energy barrier obtained following the minimum energy path between two hopping sites informs on the diffusion propensity. To test the transferability of the H_2 force fields to the study of diffusion in (oxy)hydroxides (in combination with ClayFF), the energy barriers obtained from quantum simulations for boehmite and gibbsite[6] were compared with the energy barriers obtained using classical simulations.

The energy barriers were calculated using the climbing image nudged elastic band (CI-NEB) method. Nudging forces were added to the H_2 atoms in multireplica simulations run with the nudged elastic band (NEB) method developed to identify transition states.[25,26] In an NEB simulation, each replica was connected to other replicas by inter-replica nudging forces, as detailed in ref.[25] These sets of replicas are expected to converge towards a minimum energy path (MEP) of conformational states that transition over a barrier. A spring constant for parallel and perpendicular nudging forces of 4.34 eV/Å^2 was used. Minimization was performed on each replica using the damped dynamics method from ref.[27] This minimization method requires timestep definition, and a value of 2 fs is used consistently with LAMMPS documentation stating that NEB will converge faster when the timestep is 10-fold larger than that used for MD simulations of the processes in the same system. After the regular NEB stage, the climbing image process was performed using the replica with the highest energy obtained with regular NEB, and the inter-replica forces on this replicate were converted to a force that drives its atom coordinates to the top or saddle point of the barrier. The other replicas are rearranged along the MEP to be roughly equally spaced. NEB implementation

in LAMMPS leads to approximately equally-spaced points. However, small uncertainties in the positions of these points may lead to asymmetry in the energy barrier curve when various trajectories are averaged without accounting for the variability in points along the energy curve. In the results reported, we checked for the symmetry of the curves (expected due to the crystal symmetry) and interpolated the values to equally-spaced reaction coordinates.

H_2-induced expansion

Lattice parameters were computed using NPT simulation (with independently barostated stress components). Nosé-Hoover barostat and thermostat were adopted with 100 and 1000 timesteps damping parameters, respectively. A timestep of 0.1 fs was used in 0.5 ns production runs following proper equilibration.

Simulations were performed up to the temperature of 275°C, below the typical temperatures reported for the three mineral dehydration. Boehmite starts dehydrating at 300°C.[28] Gibbsite dehydrated above (endothermic peak begins at 270°C and ends at 317°C, with a peak temperature occurring at 300°C)[29] Portlandite dehydrates above 400°C.[30] The comparison of the thermal expansion obtained with ClayFF with experimental data is discussed in the Supporting Information (Table S2).

H_2-induced expansion was evaluated by randomly introducing a number of H_2 molecules in the simulation box. Then, an NVE run followed by an NVT run was performed so that the H_2 molecules could accommodate in the preferential interstitial sites. Next, an NσT simulation, as described above, was performed to get the equilibrated lattice parameters for various temperatures.

Generalized self-diffusion

The general description of the diffusion process follows (e.g.,[31]):

$$\langle r \rangle^2 = D_\alpha t^\alpha \tag{1}$$

where $\langle r \rangle^2$ is the mean squared displacement (MSD), D_α is the generalized (or fractional) (self-)diffusion coefficient with dimensions $[length^2.time^{-\alpha}]$, t is the time, and α is the anomalous diffusion exponent. When $\alpha = 1$, diffusion is normal (Fickean). Anomalous diffusion occurs when $\alpha > 1$ (superdiffusion) or $\alpha < 1$ (subdiffusion). Herein, we adopt the following classification of subdiffusive regimes:[32] strong subdiffusion $0.4 < \alpha < 0.6$, weak subdiffusion $0.6 < \alpha < 1$. Various phenomena might lead to an anomalous diffusion regime, including fractal or viscoelastic substracts.[31] Furthermore, within the framework of continuous-time random walks, subdiffusion can result from various factors, such as increased affinity or surface-induced damping in random potentials,[33,34] asymptotic power-law waiting times, random or correlated successive waiting times, random walks in an ageing environment or under confinement, and highly damped particles in random potentials (see[31] for a comprehensive review). Subdiffusion was reported on bound water behavior on hydrophilic surfaces,[35] confined water in hydrophilic micropores,[36,37] charge carrier transport in amorphous semiconductors,[38] porous systems,[39,40] and in the dynamics of beads in polymeric networks.[38]

Getting the self-diffusion coefficient of mobile species trapped in solids from the analysis of the MSD is one strategy that has also been used to evaluate H_2 diffusion.[7] Generalized diffusion coefficients and anomalous diffusion exponent can be obtained from molecular dynamics simulations by fitting a power law to the MSD of H_2 per Cartesian direction. MSD was computed during NVE runs (to avoid the bias introduced by the fictive forces associated with thermostat and barostat[41]) following proper temperature and subsequent NVE equilibration. MSD was first computed at 25°C for one μs timescale per Cartesian direction. We considered the average of 5 independent trajectories. Four H_2 molecules per simulation box were considered. Shorter simulations (at the nanosecond timescale) were then performed for all temperatures studied. In this case, 20 trajectories were considered to compute the MSD. The Supporting information discusses the collective effects in H_2 diffusion for systems with up to ten H_2 per simulation box. The results obtained in a dilute system are statistically equivalent to those with four H_2. Uncertainty was computed from the standard deviation of

the D_α and α obtained values for each trajectory. In the post-processing, the initial ballistic regime was excluded[41] from the exponential fittings to get D_α and α values.

Results

Preferential sites and energy barriers

Snapshots of the preferential sites of H_2 in pristine boehmite, gibbsite, and portlandite are shown in Figure 1 for systems at 25°C using Köster et al.[16] force field for H_2. Simulated portlandite shows the inclined OH bonds consistently with three equivalent Wyckoff sites with partial occupancies reported for this mineral.[42] The distances between hydrogen in the H_2 and the other species (Oh and Hh, for OH group oxygen and hydrogen, respectively; Al for gibbsite and boehmite, Ca for portlandite) can be inferred from the first peak (for the first neighbor) in the radial distribution functions (RDF) shown in Figure 1. The H_2 is located above (at the Oh-Hh level) in-between two Al or Ca atoms. The Köster et al.,[16] Buch,[17] and Hirschefelder et al.[18] force fields for H_2 yield similar RDFs, whereas the Cracknell[19] force field exhibits a distinct local environment for H_2. This result is expected since the Cracknell force field is two-sites and has parameters that differ from the other three.

To verify the validity of using classical MD to model the dynamics of H_2 in (oxy)hydroxides, we compare the energy barriers obtained from DFT calculations by Shen et al.[6] in boehmite with the one obtained with classical simulations with ClayFF and the four force fields tested for H_2. The potential energy landscapes in the proximity of the H_2 preferential sites are depicted in Figure 2 for the reaction coordinate studied by Shen et al.[6] for boehmite: a reaction path within the interlayer from the preferential sites closer to the bottom Al/Ca layer to the site closer to the opposing top Al/Ca layer. The Köster et al.,[16] Buch,[17] and Hirschefelder et al.[18] force fields yield similar energy landscapes, whereas Cracknell[19] shows a fairly distinct energy landscape. This result comes from the fact that the Cracknell force field, albeit being two-sites, has a sensibly smaller Lennard-Jones diameter and potential

well depth for H.

For the reaction path shown in Figure 2, the energy barrier obtained from DFT simulations is ΔE=0.42 eV.[6] The energy barrier obtained with Köster et al.[16] (ΔE_{NEB}=0.33 $\pm$ 0.01 eV) and Hirschefelder et al.[18] (ΔE_{NEB}=0.37 $\pm$ 0.02 eV) and Buch[17] (E_{NEB}=0.33 $\pm$ 0.01 eV) are in better agreement with DFT results than Cracknell[19] (ΔE_{NEB}=0.10 $\pm$ 0.01 eV). The one-site force fields yield comparable results. In the Supporting information, the energy barriers obtained from potential energy landscape evaluation can be approximately inferred by the charts provided, and for the reaction path in Figure 2 they are to close to 0.5 eV when Köster et al. force field is used. It must be noted that CI-NEB method has a better resolution (in terms of reaction coordinate discretization), searches for the MEP of conformational states that transition over a barrier (which should deviate from the linear path depicted in the contour plots of Figure 2), and that it is developed to capture energy barriers better.

The energy barriers, evaluated along the three Cartesian directions using the CI-NEB (ΔE_{NEB}) method, are compiled in Table 1. In these simulations, the initial position in the reaction path is in a preferential site, and the final position is at the neighboring unit cell (i.e., plus a step of one unit cell vector according to the direction considered). Only the Köster et al.[16] force field for H_2 is utilized in these analyses. This choice is justified by the fact that this force field is the most recent of the tested force fields and has been developed to improve the description of thermodynamic data of H_2 in fluid mixtures. Additionally, all three tested one-site force fields yield similar energy barriers compared to DFT results, as discussed above. The energy barriers are significantly larger than the thermal energy (k_bT is on the order of 0.03 eV in the range of T considered) in all cases, corroborating the picture of H_2 being trapped or significantly slowed down in bulk (oxy)hydroxides.[3,6] The analysis of ΔE indicates that diffusion is hampered in boehmite and gibbsite compared to portlandite.

For boehmite, the energy barrier along z agrees with the value reported for the reaction path in Figure 2, as expected since this is the direction in which transfers are facilitated in boehmite's interlayer. The other interlayer direction corresponds to x in the Cartesian frame

and the respective energy barrier (1.23 eV) can be compared with the values obtained with DFT[6] of 0.86 eV for [001] crystallographic direction. Besides the difference expected from classical and quantum simulations, the difference might come from the reaction path being considered in each case not being precisely the same due to the changes in the reference frame. Note that a difference in the energy barrier of the order of a tenth of an electronvolt has been deemed reasonable in comparisons between DFT and classical simulations (e.g.,[7]). The values obtained with CI-NEB show that diffusion along x and y directions are energetically unfavored when compared with the direction along z. These results suggest a 1D diffusion response for boehmite.

The energy barrier in gibbsite reported by Shen et al.[6] for H_2 crossing Al structural layers is reported to exceed 0.77 eV. The values obtained here with CI-NEB agree with this constraint. The energy barriers obtained from DFT for reaction paths in the interlayer are > 0.70 and >1.01 eV according to the two final H_2 sites considered in Shen et al.[6] These values are consistent with our results. The energy barrier on the order of the eV might translate into limited diffusion for all three directions in gibbsite.

To the best of our knowledge, the energy barrier values for H_2 diffusion in portlandite are provided for the first time. As expected, diffusion along the x and y directions is favored in portlandite compared to diffusion across the Ca layers (z direction).

The consistency of the energy barrier obtained using classical MD with the DFT results builds confidence in using the one-site H_2 force fields combined with ClayFF to capture dihydrogen diffusion in (oxy)hydroxides.

Diffusion of H_2 up to the μs timescale

Figure 3 shows the MSD of H_2 per direction for simulated times up to the microsecond scale at 25°C in boehmite, gibbsite, and portlandite. The transition from the initial ballistic regime to the subdiffusive regime occurs at approximately 0.01 ps in all cases. Up to the microsecond scale, only diffusion along the z-axis in boehmite and along the x- and y-axes in

Table 1: Energy barrier computed from CI-NEB ΔE_{NEB} for H_2 transport in boehmite, gibbsite, and portlandite using Köster et al.[16] force field for H_2.

(Oxy)hydroxide	Direction	ΔE_{NEB} [eV]	ΔE_{NEB} [kJ/mol]
Boehmite	x (interlayer)	1.23±0.01	119±1
	y (across Al layers)	5.76±1.89	556±182
	z (interlayer)	0.32±0.01	31±1
Gibbsite	x (interlayer)	1.02±0.16	98±15
	y (interlayer)	1.57±0.65	152±63
	z (across Al layers)	1.05±0.40	101±39
Portlandite	x (interlayer)	0.36±0.09	35±9
	y (interlayer)	0.33±0.12	32±12
	z (across Ca layers)	0.52±0.03	50±3

portlandite exceeds the values corresponding to the distances between the endpoints of the NEB calculations. In gibbsite, this does not occur. These results support the interpretation of 1D and 2D diffusion for boehmite and portlandite, respectively, while H_2 remains effectively trapped in gibbsite for at least several microseconds, based on the trends observed in the MSD. The distances between the endpoints of the NEB calculations are on the order of the unit cell vector length in the x and z directions in boehmite, x and y directions in portlandite, and in the y direction in gibbsite. For the other directions, the NEB distance exceeds at least twice the corresponding unit cell vector length, meaning that a significantly more tortuous path is required for diffusion along these directions.

The figure also shows the parameters D_α and α computed as a function of the timescale. The values of α for boehmite and portlandite converge for timescales above roughly 500 ns, while the α of gibbsite shows an increasing trend. The dynamics remain strongly subdiffusive with α not exceeding 0.6 for most cases, except for diffusion along the z direction in boehmite. The D_α values show an overall decreasing trend, except for the y direction in portlandite, where a marked fluctuation is observed. The increasing trend of α as a function of the timescale in gibbsite is to some extent compensated by the decrease in D_α. The graphics on the right show that in most cases D_α decreased with increasing α values for the three minerals. These results show that subdiffusion persists at least up to the microsecond scale in the (oxy-)hydroxides studied. Extrapolation of the observed trends suggests that subdiffusion

should persist to larger timescales.

Temperature dependence of diffusion

To evaluate the temperature dependence of diffusion parameters, simulations at various temperatures were performed up to the nanosecond scale. As can be observed in Figure 3, this timescale is statistically representative of the behavior up to the microsecond timescale (considering that the uncertainty in the values reported in this figure is on the order of 0.1 for α and 0.01 $\text{Å}^2/\text{ps}^\alpha$ for D_α). In the Supporting Information, we show that D_α and α obtained from the simulation up to the microsecond timescale at 25°C can be compared to the values calculated from the simulation up to the nanosecond when one accounts for the standard error on D_α and α.

The generalized self-diffusion coefficient D_α and anomalous exponent α of H_2 in boehmite, gibbsite, and portlandite are shown in Figure 4 as a function of temperature. Dynamics are subdiffusive in all cases and can be classified as strong subdiffusion with $\alpha < 0.6$,[32] except for a few points in portlandite and the z direction in boehmite for which a weak subdiffusion is observed. Anisotropy in diffusion is marked, particularly in boehmite and in portlandite to a lower extent. In portlandite, both directions parallel to the calcium plane show larger α; in boehmite, one direction parallel to the aluminum plane shows a markedly larger α for temperatures above 100°C. Similar conclusions can be reached when analyzing D_α for boehmite. These results suggest that diffusion in portlandite is mostly 2D (dominated by migration in the interlayer directions parallel to the Ca plan) and mostly 1D in boehmite (dominated by migration in the z direction, in the interlayer parallel to the Al plan). The very low values of D_α and α for gibbsite indicate that H_2 hardly diffuses in this mineral. These results are consistent with the energy barrier computed with the CI-NEB method.

Both generalized diffusion coefficients and anomalous diffusion exponents increase approximately linearly with temperature in the range studied. In this context, a simple Arrhenius-like thermal activation is insufficient to capture the temperature dependence due

to the temperature increase of α. The linear fit parameters of the points in Figure 4 are given in Table 2. In the Supporting Information, we show how the logarithm of α, D_α, and the MSD as $t \to \mu$s (i.e., αD_α) evolves with $1/T$. Linear trends can be identified in some cases, but unequivocal trends cannot be established.

Both generalized diffusion coefficients and anomalous diffusion exponents increase approximately linearly with temperature in the range studied. The linear fit parameters of the points in Figure 4 are given in Table 2. In this context, a simple Arrhenius-like thermal activation cannot be applied directly to D_α due to its quasi-property nature (i.e., this property is defined by a ratio of physical quantities, length, and time, with non-integer exponents[43]). In the Supporting Information, we show how the logarithms of α and D_α evolve with $1/T$. While linear trends can be identified in some cases, unequivocal trends cannot be established. To obtain an activation energy, we define a timescale-dependent diffusion coefficient using an Einstein-like equation:

$$D_{t\to\tau} = \lim_{t\to\tau} \frac{\mathrm{MSD}(t)}{t} = \lim_{t\to\tau} D_\alpha t^{\alpha-1} \tag{2}$$

where τ corresponds to the timescale considered. To maintain consistency with Eq. 1, we have not included the $1/(6d_s)$ factor, where d_s is the dimensionality, in the right-side in the equation above. This diffusion coefficient has the usual dimension of a diffusion coefficent. Arrhenius plots of $D_{(t\to\tau)}$ are provided in Figure S6 in the Supporting Information for a timescale of τ=1 μs and considering a 1/6 factor multiplied to $D_{t\to\tau}$ per direction. The Arrhenius activation energy E_a can therefore be defined for H_2 in the systems studied using $D_{t\to\tau}$. Anomalous diffusion described by a power law leads to an activation energy that depends on the timescale τ. This dependence is shown in Figure S6 in the Supporting Information, and follows a logarithmic trend. Thus, E_a does not converge to a single value as the timescale increases, but rather grows slowly with the timescale considered. The activation energies are also dependent on the direction considered, as expected from the analysis of energy barriers from NEB simulations. The comparison of E_a with the energy barriers

obtained from NEB simulations shows good agreement for boehmite along the diffusing direction (z direction). The activation energies computed from $D_{t\to\tau}$ in the non-diffusing directions (x and y) are much lower than the energy barriers obtained from NEB. This occurs because the movement of H_2 molecules is restricted to the interstitial basins in these directions, where the molecules do not cross the energy barriers computed by NEB. In the basins, the molecules move with fewer constraints, leading to a much lower E_a when considering only the MSD compared to NEB. A similar reasoning applies to the diffusing (x and y) and non-diffusing (z) directions in portlandite. In portlandite, the activation energies obtained from NEB and MSD differ to a more pronounced extent, with differences on the order of 10-20 kJ/mol. It must be noted that the standard deviations of NEB energy barriers are on the order of 10 kJ/mol, and uncertainty is also expected from the linear fitting of Arrhenius plots of E_a obtained from MSD. Given these uncertainties and the fact that MSD and NEB simulations are performed using different techniques (molecular dynamics and energy minimization, respectively), the results can be considered fairly consistent. No direct comparison of MSD and NEB activation energies is provided for gibbsite, as there is no diffusing direction in this system.

Table 2: Linear fits ($y = AT + B$) of anomalous exponent α and generalized self-diffusion coefficient D_α per direction obtained from Figure 4.

		α			D_α		
	dir.	A[1/°C]	B [-]	R^2	A [Å^2/(ps$^\alpha$.°C)]	B [Å^2/(ps$^\alpha$)]	
Boehmite	x	4.72E-5	2.46E-3	0.19	4.82E-5	-2.38E-3	0.70
	y	-2.77E-4	4.36E-1	0.15	8.88E-5	1.23E-2	0.60
	z	1.88E-3	-1.58E-1	0.78	7.76E-4	-2.14E-1	0.64
Gibbsite	x	6.05E-4	-1.30E-1	0.60	4.99E-4	-1.33E-1	0.85
	y	7.61E-4	-1.87E-1	0.72	4.46E-4	-9.34E-2	0.76
	z	1.03E-3	-2.50E-1	0.82	3.26E-4	-6.89E-2	0.93
Portlandite	x	7.70E-4	2.05E-1	0.82	1.65E-3	-4.27E-1	0.80
	y	3.38E-4	3.73E-1	0.33	1.07E-3	-1.88E-1	0.83
	z	1.01E-3	-4.29E-2	0.92	8.38E-4	-1.66E-1	0.97

To quantify the mobility of H_2 in the three minerals, we compute a characteristic time $t_{nm} = (1\ \text{nm}^2/D_\alpha)^{(1/\alpha)}$ for a mean displacement of one nanometer and for a mean displace-

ment of one micrometer $t_{\mu m} = ((1000\text{ nm})^2/D_\alpha)^{(1/\alpha)}$. The results are plotted in Figure 5 for portlandite, gibbsite, and boehmite. The timescale assocaited to micrometer scale are several orders of magnitude larger than those for the nanometer scale, in particular for low α, due to the $(1/\alpha)$ scaling. The diffusion along x in boehmite is extremely slowed down consistently with the diffusion coefficient and α value reported in Figure 4 for all temperature tested. The results for gibbsite exceed experimentally (reasonably) accessible timescales even when one considers the nanometer scale for temperatures below roughly 100°C. The comparison of t_{nm} and $t_{\mu m}$ for portlandite suggests that H_2 occasionally produced within the bulk crystal has time to escape the nanometric crystal in a short timescale, while a much larger observation time would be needed to observe the same H_2 release in micrometric-sized particles. This point is important to understand how the H_2 produced in nanometric portlandite particles[5] might be compared with the delayed release of H_2 in cement systems, in which portlandite might appear as micrometer-sized inclusions. These observations corroborate the picture in which pristine gibbsite allows virtually no diffusion of H_2, whereas boehmite and portlandite exhibit anisotropic diffusion that can be measured within experimentally accessible timescales. These results further support the conclusion that H_2 migration across the Al layers in gibbsite (for temperature below 150 °C) is unlikely. In contrast, crossing the Ca layer in portlandite is achievable within experimentally accessible timescales, although diffusion along this direction is significantly slower compared to the interlayer direction. The relevance of subdiffusion for the minerals studied here should be considered as a function of timescales (and associated length scales) of interest. Even in the case of nanometer-sized particles of these minerals, our results suggest that subdiffusion should play a significant role in H_2 dynamics.

H_2-induced expansion and collective effects

Figure 6 (left) shows that the introduction of H_2 in the (oxy)hydroxides studied leads to a linear expansion up to at least N =10 H_2 molecules per simulation box for boehmite (i.e.,

N_H=10/(7x2x6) per unit cell). The same is observed for portlandite (i.e., N_H=10/(6x6x6) per unit cell), except for the case of 125°C. With gibbsite, the linear domain decreases when the temperature increases, persisting up to at least N =10 molecules per simulation box (i.e., N_H=10/(3x4x2) per unit cell) at 25°C and N =5 for 125°C. The coefficient of H_2-induced dilatation α^H per number of H_2 molecules N_H in a unit cell is computed in the range of linear H_2-induced dilatation with:

$$\alpha^H = \frac{1}{V_0}\frac{dV(T)}{dN_H} \tag{3}$$

adopting as reference volume $V_0 = V(T$ =25°C). The results per direction are computed using a similar definition with the values of reference (a_0, b_0, and c_0) being also taken at 25°C. The results are shown in Figure 6 (right). The expansion in gibbsite is roughly isotropic (all directions contributing equally). The main contribution to expansion occurs in the c direction in portlandite, in agreement with experiments.[8] Directions a and b are the main contributors to boehmite expansion, which is slightly compensated by a contraction in c direction.

In the Supporting Information, we show that the deviation from linear volume expansion is related to an increase in interlayer distances (associated with a loss of layer-layer cohesion) in the case of boehmite and likely portlandite. In the case of gibbsite, the steep increase in volume with temperature and H_2 content is due to amorphization (this observation needs to be confirmed with future studies using reactive force fields). Local amorphization in the vicinity of H_2 molecules is also observed in portlandite.

Collective effects in diffusion among H_2 molecules are discussed in the Supporting Information. Up to at least N=10 H_2 molecules per simulation box, both α and D_α show no statistically significant differences when plotted as a function of N. This result corroborates the picture of a dilute system in which no significant collective effects among H_2 molecules are present. The discussion in this section shows that the dilation of (oxy)hydroxides induced by the presence of H_2 does not lead to any significant increase in H_2 diffusion for

the concentration and temperature range considered. Of course, this conclusion is valid for pristine crystals (i.e., in the absence of radiation-induced damage).

Discussion on the nature of subdiffusion

In this section, we discuss the possible physical origins of the subdiffusive behavior observed in the (oxy-)hydroxides. In the literature, the physical origins of subdiffusive behavior are often attributed to the significant residence times of H_2 in interstitial sites and confinement in "cages" or energy basins within these sites. Among the various processes leading to subdiffusion,[31] random walks interrupted by random waiting times are known to be subdiffusive.[44] Particles moving in the vicinity of solid surfaces have been shown to exhibit subdiffusive to superdiffusive behavior depending on the potential and dissipation or damping parameter.[33] In this context, superdiffusion is related to low damping, leading to shorter residence times, while subdiffusion is associated with strongly damped dynamics, resulting in longer residence times.[33] Among the various mechanisms proposed to explain subdiffusion (see Section "Generalized Self-Diffusion"), we explore whether the one related to damped particles diffusing in random potentials explains the subdiffusion of H_2 in (oxy-)hydroxides.

A key element to validate is the relevance of considering the studied systems as yeilding a random potential landscape for diffusing H_2. Lacasta et al.[33] observed subdiffusive dynamics only in random potential landscapes, while diffusion in periodic potential landscapes remained Fickean. Other authors have also reported subdiffusive behavior in overdamped particle diffusion in random potentials.[34] In crystalline systems like the ones studied here, the distances between hopping sites should be approximately constant. However, due to thermal fluctuations, some variability in these distances occurs. The analysis of the total reaction coordinate from NEB simulations shows variability, with coefficients of variation for the length in boehmite on the order of 1% along the x and y directions, and exceeding 15% for the z direction; in gibbsite and portlandite, all coefficients of variation are above 15%.

Local disorder can be visualized in the potential energy landscape charts in the Supporting Information. These arguments allow us to conclude that the potential energy landscapes of the three (oxy-)hydroxides studied at the temperatures tested differ to some extent from a perfectly periodic landscape and can be approximated as random potentials when accounting for thermal fluctuations that lead to local disorder.

The second element to define is how the dynamics are damped. In our simulations, damping is controlled by adjusting the Lennard-Jones potential well ϵ_{HH} value of H_2 in the force field. This adjustment is modulated by a dimensionless factor γ, so that the damped Lennard-Jones potential well parameter $\epsilon^{damp}HH$ can be expressed as a function of the undamped parameter ϵHH: $\epsilon^{damp}HH = \gamma\epsilon HH$. Since the Lorentz-Berthelot combining rules are applied, changing ϵ^{damp}_{HH} also alters the interactions with all other atoms in the system (we show these changes in the Lennard-Jones potential for all atoms in the system for selected values of γ in the Figure S9 in the Supporting Information). We performed simulations at 25°C with various γ values, covering overdamped ($\gamma > 1$), non-damped ($\gamma = 1$), and underdamped ($\gamma < 1$) conditions. Köster et al.'s[16] one-site force field was used.

Figure 7 shows the MSD of H_2 per direction in boehmite, gibbsite, and portlandite at 25°C, considering two damping parameters: $\gamma = 10$ (overdamped) and 1/1000 (underdamped). Overdamped dynamics lead to increased subdiffusion, while the underdamped case results in accelerated dynamics compared to the original Köster et al.[16] H_2 force field in all three minerals, with superdiffusion (MSD scaling approximately as t^2) observed in portlandite for diffusion along the x and y directions.

The anomalous diffusion parameter α is plotted as a function of γ in Figure 8. With decreasing γ, the diffusional behavior exhibits the following changes: (i) in boehmite, it transitions from subdiffusive (overdamped) to Fickean along the z direction; (ii) in gibbsite, it becomes less subdiffusive in a roughly isotropic manner; and (iii) in portlandite, it reaches superdiffusive behavior along the x and y directions. The entire range of behavior, from subdiffusive to superdiffusive, can be achieved by controlling the γ coefficient, which can be

interpreted as the affinity of the H_2 molecules with respect to the bulk crystal. This effect can also be obtained by increasing the temperature, which leads to greater thermal fluctuations, allowing energy barriers to be more easily overcome in a shorter time, thus accelerating the dynamics, as discussed in the previous sections. These observations show that a key element explaining the subdiffusion of H_2 in the (oxy-)hydroxides studied is the higher affinity of H_2 to the mineral in their interstitial sites.

To relate damping with residence times, we compute the distribution of residence times per direction for the underdamped system in 6 ns-long trajectories (in this timescale, non-damped and overdamped simulations would not yield enough jumps to provide good statistics). Displacement of H_2 particles is recorded every 1 ps, and a jump is counted whenever a displacement between two recorded times exceeds the length of the lattice vector in the considered direction. In Figure S10 in the Supporting Information, we show that increasing underdamping (i.e., decreasing γ) results in a distribution of residence times with increased frequencies of longer residence times. This long-tail distribution for the residence times affects the apparent diffusion by making low frequency jumps significant. The usual law describing lattice diffusion in solids reads (e.g., [45]):

$$D = \lambda^2 \nu \exp \frac{-E_a}{RT} = \frac{1}{z} \lambda^2 \Gamma \tag{4}$$

where λ is the jump distance, $\Gamma = z\nu \exp[-E_a/RT]$ is the jump frequency, ν is the vibrational frequency of the molecules, and z is the number of nearest neighboring interstitial sites. The jump distance is approximately constant, with some variability expected under finite temperature, as discussed above. The number of neighboring sites is also constant. We evaluate the vibrational frequency of H_2 in the simulations by calculating the vibrational density of states (VDOS) from the velocity autocorrelation function (as detailed in the Supporting Information). The average values are 1420 cm^{-1} for boehmite, 670 cm^{-1} for gibbsite, and 717 cm^{-1} for portlandite, with a standard deviation on the order of hundreds

of cm^{-1}. For comparison, the values reported by Shen et al.[6] are close to 1500 cm^{-1} for boehmite and 1000 cm^{-1} for gibbsite, also with large variability in the frequencies. This parameter changes insignificantly with γ in gibbsite and portlandite when considering the variability within the frequency band; in boehmite, the average frequency increases with decreasing γ. Therefore, the main parameter affecting the distribution of the jump frequency must be the activation energy. In Figure S13, we show that the CI-NEB energy barrier decreases in an exponential-like fashion with decreasing γ. Lower values of activation energy should be associated with shorter residence times.

The results above show that decreasing the affinity of H_2 with the crystal surfaces via γ is insufficient to transition from subdiffusive to normal and then superdiffusive behavior in all directions in the three (oxy)hydroxides studied. The direction across Al and Ca layers remains subdiffusive even with very low γ. Channel sizes within the bulk crystals and the connectivity of interstitial sites should be considered to explain the anisotropy in diffusion in the minerals studied.

The discussion by Lacasta et al.[33] suggests that superdiffusive behavior in underdamped particles diffusing on a random potential is likely transient. Conversely, the same authors point out that subdiffusion may not be transient (but rather an actual asymptotic behavior) due to multiple trapping, particularly at low temperatures. These arguments support the interpretation of the results in our study, suggesting that subdiffusion in the (oxy)hydroxides should persist beyond the microsecond scale.

The conclusion of the numerical experiments in this section is that the affinity of H_2 with the interstitial sites in the (oxy)hydroxides studied explains the damped dynamics resulting in subdiffusion. However, these effects are limited by the energy barriers, which occur anisotropically due to the layered structure of the materials. This discussion corroborates arguments from the literature that subdiffusion should not be transient in the bulk minerals studied. This result suggests that screening other minerals for H_2 (sub)diffusion can be done by the evaluation of energy barriers (associated with molecular affinity to the solid) without

the need for simulating long trajectories.

Conclusion

The dynamics of H_2 in three (oxy)hydroxides relevant for energy production - boehmite, gibbsite, and portlandite - were quantified using classical molecular simulations. The dilation of the crystalline lattice due to thermal expansion and H_2 introduction were explicitly considered in the simulations. We conclude:

- *On using classical molecular dynamics to assess H_2 in three (oxy)hydroxides.* The energy barriers obtained with one-site force fields for H_2 combined with ClayFF are approximately consistent with those obtained from quantum calculations in gibbsite and boehmite.[6] This builds confidence in using classical simulations to evaluate H_2 dynamics within other (oxy)hydroxides (clays, phases in cement systems, geomaterials, etc.) for future work. Classical simulation enables assessing the timescales needed to evaluate dynamics (up to the microsecond scale). Köster et al.[16] and Hirschefelder et al.[18] force fields for H_2 yield a better comparison with CI-NEB DFT calculations in the case of boehmite. The Cracknell[19] force field favors faster dynamics, leading to a significantly different energy landscape compared to the other force fields. These differences are due to the smaller Lennard-Jones diameter and potential well depth for H in the Cracknell[19] force field.

- *On the anisotropic subdiffusive dynamics of H_2.* H_2 dynamics in the three (oxy)hydroxides is subdiffusive, with anomalous diffusion exponent $\alpha < 0.9$ in all cases.[32] Subdiffusion persists at least up to the microsecond scale. The origins of subdiffusion in the three (oxy)hydroxides can be linked to confinement in "cages" or energy basins in the interstitial sites. The relevance of subdiffusion for the minerals studied here should be considered as a function of timescales (and associated length scales) of interest. In the case of nanometer-sized particles of these minerals, our results suggest that subdiffusion

should play a significant role in H_2 dynamics. The dynamics are markedly anisotropic: as expected in layered (oxy)hydroxides, crossing the Al/Ca layers is energetically unfavorable, and most of the diffusion occurs in the interlayer. Generalized diffusion per direction with subdiffusive anomalous exponent captures the pronounced anisotropies in minerals studied. Diffusion of H_2 differs in these minerals, with H_2 being effectively trapped in gibbsite, showing a 1D diffusion in boehmite and a 2D diffusion in portlandite. Both generalized diffusion coefficients and anomalous diffusion exponents are temperature-dependent but Arrhenius-like thermal activation cannot be applied directly to these parameters. The definition of a time-dependent diffusion coefficient allows for the calculation of an activation energy that agrees with the magnitude of the energy barrier obtained using CI-NEB along the diffusing directions (z in boehmite, and x and y in portlandite).

- *On the nature of subdiffusion of H_2 in (oxy)hydroxides.* The affinity of H_2, modulated by its interaction with other species in the solid, results in subdiffusive behavior in the (oxy)hydroxides studied. Our results suggest that the relatively high energy barriers that H_2 must overcome to jump between interstitial sites lead to a distribution of residence times with long, fat tails in the direction of longer residence times. This phenomenon should be associated with subdiffusive behavior. By adjusting the H_2 Lennard-Jones potential well value, one can observe transitions from subdiffusive to Fickean and even superdiffusive in underdamped cases in some direction in the (oxy)hydroxides studied. However, diffusion across Al and Ca layers remains subdiffusive irrespective of H_2 Lennard-Jones potential well value changes, indicating that channel sizes and interstitial site connectivity also play roles in diffusion anisotropy. Subdiffusion is likely to persist beyond the microsecond scale, especially at low temperatures, due to multiple trapping effects.

- *On the H_2-induced dilatation.* The crystal structure of the three (oxy)hydroxides dilates

linearly with the number of H_2 molecules introduced up to 4 to 5 per simulation box (the simulation boxes studied have a volume on the order of 10 nm^3). Dilation perpendicular to the Al/Ca layers is the main contribution to the volumetric expansion. The expansion of (oxy)hydroxides induced by the presence of H_2 leads to no significant increase in H_2 diffusion for the concentration and temperature range considered. Of course, this conclusion is valid for systems in the absence of radiation-induced damage.

This work has broad implications for the safety of nuclear waste disposal systems. In order to have safer systems, it is essential to be able to model the dihydrogen formation and transport in the material over long periods of time. The simulations carried out in this work provide a basis for modeling the transport part, i.e., the diffusion of H_2 within the mineral studied, and thus for being more precise about the evolution of H_2 release over time. Diffusion of H_2 can be studied in other solid phases relevant to nuclear waste disposal systems using the same strategy as that proposed in this study. Further studies will also focus on elucidating the formation processes in other minerals of interest for nuclear waste disposal. The results above corroborate that transport properties might provide elements to understand the differences in delayed H_2 production in (oxy)hydroxides. Furthermore, anomalous subdiffusive behavior requires a theoretical treatment in a framework that goes beyond Fickian diffusion. In this context, generalizations of Fick's law using fractal or fractional derivatives can be applied.[31] Future work can extend the analysis of diffusion to other species in (oxy)hydroxides.

Supporting Information Available

"Supporting Information: H_2 Anisotropic Subdiffusion and Induced Expansion in Portlandite, Gibbsite and Boehmite"

References

(1) LaVerne, J. A.; Tandon, L. H $_2$ and Cl $_2$ Production in the Radiolysis of Calcium and Magnesium Chlorides and Hydroxides. *The Journal of Physical Chemistry A* **2005**, *109*, 2861–2865.

(2) Le Caër, S.; Dezerald, L.; Boukari, K.; Lainé, M.; Taupin, S.; Kavanagh, R. M.; Johnston, C. S. N.; Foy, E.; Charpentier, T.; Krakowiak, K. J.; Pellenq, R. J. M.; Ulm, F. J.; Tribello, G. A.; Kohanoff, J.; Saúl, A. Production of H2 by water radiolysis in cement paste under electron irradiation: A joint experimental and theoretical study. *Cement and Concrete Research* **2017**, *100*, 110–118.

(3) Kaddissy, J. A.; Esnouf, S.; Durand, D.; Saffre, D.; Foy, E.; Renault, J.-P. Radiolytic Events in Nanostructured Aluminum Hydroxides. *The Journal of Physical Chemistry C* **2017**, *121*, 6365–6373.

(4) Jones, B. M.; Aleksandrov, A. B.; Zhang, X.; Rosso, K. M.; LaVerne, J. A.; Orlando, T. M. Electron-Stimulated Formation and Release of Molecular Hydrogen and Oxygen from Boehmite Nanoplatelet Films. *The Journal of Physical Chemistry C* **2022**, *126*, 2542–2547.

(5) Herin, T.; Charpentier, T.; Bouniol, P.; Le Caër, S. Behavior of Portlandite upon Exposure to Ionizing Radiation: Evidence of Delayed H2 Production. *The Journal of Physical Chemistry C* **2023**, *127*, 20245–20254.

(6) Shen, Z.; Ilton, E. S.; Prange, M. P.; Mundy, C. J.; Kerisit, S. N. Diffusion Mechanisms of Radiolytic Species in Irradiated Al (Oxy-)Hydroxides. *The Journal of Physical Chemistry C* **2018**, *122*, 28990–28997.

(7) Onwudinanti, C.; Pols, M.; Brocks, G.; Koelman, V.; van Duin, A. C. T.; Morgan, T.; Tao, S. A ReaxFF Molecular Dynamics Study of Hydrogen Diffusion in Ruthenium–The Role of Grain Boundaries. *The Journal of Physical Chemistry C* **2022**, *126*, 5950–5959.

(8) de Noirfontaine, M.-N.; Acher, L.; Courtial, M.; Dunstetter, F.; Gorse – Pomonti, D. An X-ray powder diffraction study of damage produced in Ca(OH)2 and Mg(OH)2 by electron irradiation using the 2.5 MeV SIRIUS accelerator. *Journal of Nuclear Materials* **2018**, *509*, 78–93.

(9) Dwivedi, S. K.; Vishwakarma, M. Hydrogen embrittlement in different materials: A review. *International Journal of Hydrogen Energy* **2018**, *43*, 21603–21616.

(10) Liu, J.; Wang, S.; Javadpour, F.; Feng, Q.; Cha, L. Hydrogen Diffusion in Clay Slit: Implications for the Geological Storage. *Energy & Fuels* **2022**, *36*, 7651–7660.

(11) Christensen, A. N.; Lehmann, M. S.; Convert, P. Deuteration of Crystalline Hydroxides. Hydrogen Bonds of gamma-AlOO(H,D) and gamma-FeOO(H,D). *Acta Chemica Scandinavica* **1982**, *36a*, 303–308.

(12) Saalfeld, H.; Wedde, M. Refinement of the crystal structure of gibbsite, A1(OH)3. *Zeitschrift für Kristallographie - Crystalline Materials* **1974**, *139*, 129–135.

(13) Henderson, D. M.; Gutowsky, H. S. A nuclear magnetic resonance determination of the hydrogen positions in Ca(OH)21. *American Mineralogist* **1962**, *47*, 1231–1251.

(14) Cygan, R. T.; Greathouse, J. A.; Kalinichev, A. G. Advances in Clayff Molecular Simulation of Layered and Nanoporous Materials and Their Aqueous Interfaces. *The Journal of Physical Chemistry C* **2021**, *125*, 17573–17589.

(15) Cygan, R. T.; Liang, J.-J.; Kalinichev, A. G. Molecular Models of Hydroxide, Oxyhydroxide, and Clay Phases and the Development of a General Force Field. *The Journal of Physical Chemistry B* **2004**, *108*, 1255–1266.

(16) Köster, A.; Thol, M.; Vrabec, J. Molecular Models for the Hydrogen Age: Hydrogen, Nitrogen, Oxygen, Argon, and Water. *Journal of Chemical & Engineering Data* **2018**, *63*, 305–320.

(17) Buch, V. Path integral simulations of mixed para-D2 and ortho-D2 clusters: The orientational effects. *The Journal of Chemical Physics* **1994**, *100*, 7610–7629.

(18) Hirschefelder, J.; Curtiss, C. F.; Bird, R. B. *Molecular theory of gases and liquids*, john wiley and sons ed.; 1954; pp 1110–1112.

(19) F. Cracknell, R. Molecular simulation of hydrogen adsorption in graphitic nanofibres. *Physical Chemistry Chemical Physics* **2001**, *3*, 2091–2097.

(20) Broom, D. P. et al. Outlook and challenges for hydrogen storage in nanoporous materials. *Applied Physics A* **2016**, *122*, 151.

(21) Thornton, A. W.; Simon, C. M.; Kim, J.; Kwon, O.; Deeg, K. S.; Konstas, K.; Pas, S. J.; Hill, M. R.; Winkler, D. A.; Haranczyk, M.; Smit, B. Materials Genome in Action: Identifying the Performance Limits of Physical Hydrogen Storage. *Chemistry of Materials* **2017**, *29*, 2844–2854.

(22) Rafii-Tabar, H. Computational modelling of thermo-mechanical and transport properties of carbon nanotubes. *Physics Reports* **2004**, *390*, 235–452.

(23) Du, H.; Li, J.; Zhang, J.; Su, G.; Li, X.; Zhao, Y. Separation of Hydrogen and Nitrogen Gases with Porous Graphene Membrane. *The Journal of Physical Chemistry C* **2011**, *115*, 23261–23266.

(24) Thompson, A. P.; Aktulga, H. M.; Berger, R.; Bolintineanu, D. S.; Brown, W. M.; Crozier, P. S.; in 't Veld, P. J.; Kohlmeyer, A.; Moore, S. G.; Nguyen, T. D.; Shan, R.; Stevens, M. J.; Tranchida, J.; Trott, C.; Plimpton, S. J. LAMMPS - a flexible simulation tool for particle-based materials modeling at the atomic, meso, and continuum scales. *Computer Physics Communications* **2022**, *271*, 108171.

(25) Henkelman, G.; Uberuaga, B. P.; Jónsson, H. A climbing image nudged elastic band

method for finding saddle points and minimum energy paths. *The Journal of Chemical Physics* **2000**, *113*, 9901–9904.

(26) Henkelman, G.; Jónsson, H. Improved tangent estimate in the nudged elastic band method for finding minimum energy paths and saddle points. *The Journal of Chemical Physics* **2000**, *113*, 9978–9985.

(27) Sheppard, D.; Terrell, R.; Henkelman, G. Optimization methods for finding minimum energy paths. *The Journal of Chemical Physics* **2008**, *128*, 134106.

(28) Huestis, P. L.; Graham, T. R.; Mergelsberg, S. T.; LaVerne, J. A. Identification of Radiolytically-Active Thermal Transition Phases in Boehmite. *Thermochimica Acta* **2020**, *689*, 178611.

(29) Zhu, B.; Fang, B.; Li, X. Dehydration reactions and kinetic parameters of gibbsite. *Ceramics International* **2010**, *36*, 2493–2498.

(30) Bai, T. B.; Koster van Groos, A. F.; Guggenheim, S. Phase transition, dehydration, and melting relationships of portlandite. *American Mineralogist* **1994**, *79*, 1223–1226.

(31) Metzler, R.; Jeon, J.-H.; Cherstvy, A. G.; Barkai, E. Anomalous diffusion models and their properties: non-stationarity, non-ergodicity, and ageing at the centenary of single particle tracking. *Physical Chemistry Chemical Physics* **2014**, *16*, 24128–24164.

(32) Burnecki, K.; Kepten, E.; Garini, Y.; Sikora, G.; Weron, A. Estimating the anomalous diffusion exponent for single particle tracking data with measurement errors - An alternative approach. *Scientific Reports* **2015**, *5*, 11306.

(33) Lacasta, A. M.; Sancho, J. M.; Romero, A. H.; Sokolov, I. M.; Lindenberg, K. From subdiffusion to superdiffusion of particles on solid surfaces. *Physical Review E* **2004**, *70*, 051104.

(34) Romero, A. H.; Sancho, J. M. Brownian motion in short range random potentials. *Physical Review E* **1998**, *58*, 2833–2837.

(35) Gallo, P. et al. Advances in the study of supercooled water. *The European Physical Journal E* **2021**, *44*, 143.

(36) Youssef, M.; Pellenq, R. J.-M.; Yildiz, B. Glassy Nature of Water in an Ultraconfining Disordered Material: The Case of Calcium-Silicate-Hydrate. *Journal of the American Chemical Society* **2011**, *133*, 2499–2510.

(37) Honorio, T.; Carasek, H.; Cascudo, O. Water self-diffusion in C-S-H: Effect of confinement and temperature studied by molecular dynamics. *Cement and Concrete Research* **2022**, *155*, 106775.

(38) Metzler, R.; Klafter, J. The random walk's guide to anomalous diffusion: a fractional dynamics approach. *Physics Reports* **2000**, *339*, 1–77.

(39) Mokhtari, Z.; Zippelius, A. Dynamics of Active Filaments in Porous Media. *Physical Review Letters* **2019**, *123*, 028001.

(40) Theeyancheri, L.; Chaki, S.; Bhattacharjee, T.; Chakrabarti, R. Migration of active rings in porous media. *Physical Review E* **2022**, *106*, 014504.

(41) Maginn, E. J.; Messerly, R. A.; Carlson, D. J.; Roe, D. R.; Elliot, J. R. Best Practices for Computing Transport Properties 1. Self-Diffusivity and Viscosity from Equilibrium Molecular Dynamics [Article v1.0]. *Living Journal of Computational Molecular Science* **2019**, *1*, 6324–6324, Number: 1.

(42) Desgranges, L.; Grebille, D.; Calvarin, G.; Chevrier, G.; Floquet, N.; Niepce, J.-C. Hydrogen thermal motion in calcium hydroxide: Ca(OH)2. *Acta Crystallographica Section B* **1993**, *49*, 812–817.

(43) Jaishankar, A.; McKinley, G. H. Power-law rheology in the bulk and at the interface: quasi-properties and fractional constitutive equations. *Proceedings of the Royal Society A: Mathematical, Physical and Engineering Sciences* **2013**, *469*, 20120284.

(44) Montroll, E. W.; Weiss, G. H. Random Walks on Lattices. II. *Journal of Mathematical Physics* **1965**, *6*, 167–181.

(45) Heitjans, P.; Kärger, J. *Diffusion in Condensed Matter: Methods, Materials, Models*; Springer Science & Business Media, 2006.

TOC Graphic

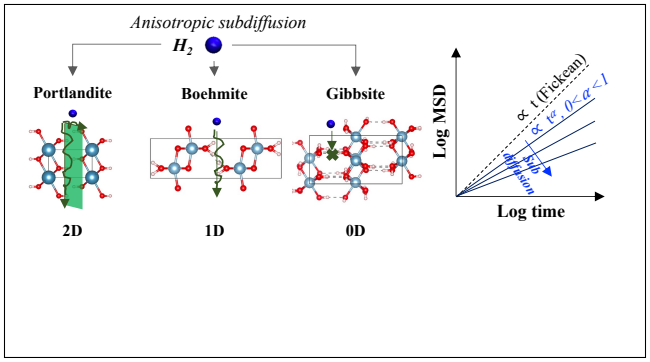
Anisotropic subdiffusion
H_2
Portlandite
Boehmite
Gibbsite
2D
1D
0D
Log MSD
Log time
∝ t (Fickean)
∝ t^α, 0<α<1
sub diffusion

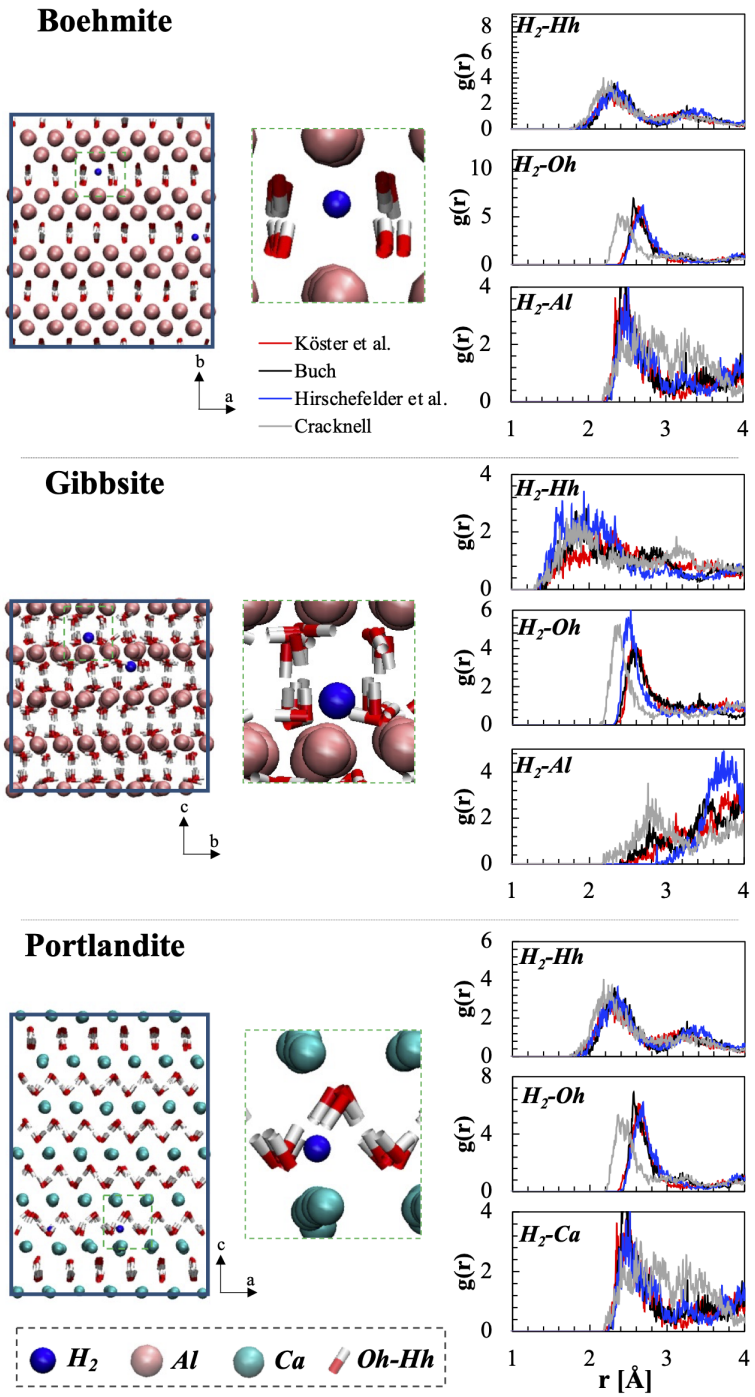

Figure 1: Snapshots of the preferential sites of H_2 in boehmite, gibbsite and portlandite using Köster et al.[16] one-site force field for H_2. At the center, we zoom in on the local environment of H_2. Radial distribution functions of H-(Al,Ca), H-Hh, and H-Oh pairs according to Köster et al.,[16] Buch,[17] Hirschefelder et al.,[18] and Cracknell[19] force fields for H_2. All simulations were performed at 25°C. Crystallographic and Cartesian frames are indicated. In gibbsite and portlandite c vector is perpendicular to the Al and Ca planes, respectively, whereas in boehmite b vector is perpendicular to the Al plane.

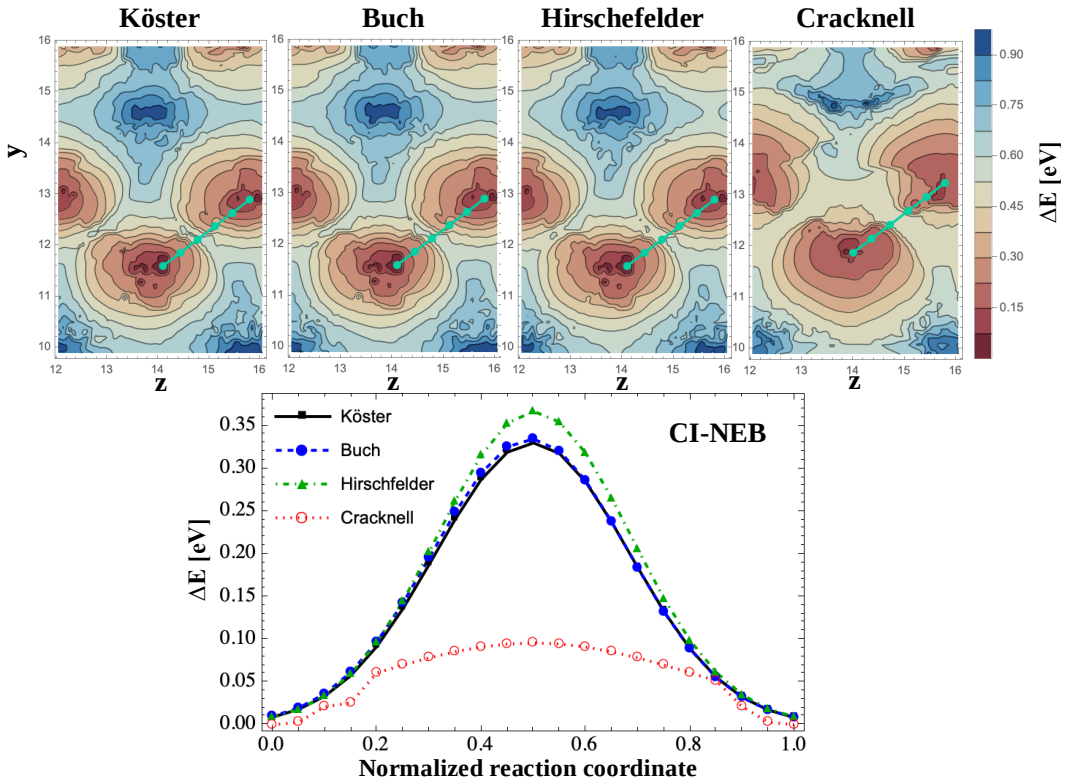

Figure 2: At top, contour plots of the variation of potential energy ΔE landscape of H_2 in **boehmite** in the yz plane intersecting a preferential site: comparison of Köster et al.,[16] Buch,[17] Hirschefelder et al.,[18] and Cracknell[19] force fields for H_2. At bottom, energy barriers evaluated by the CI-NEB method.

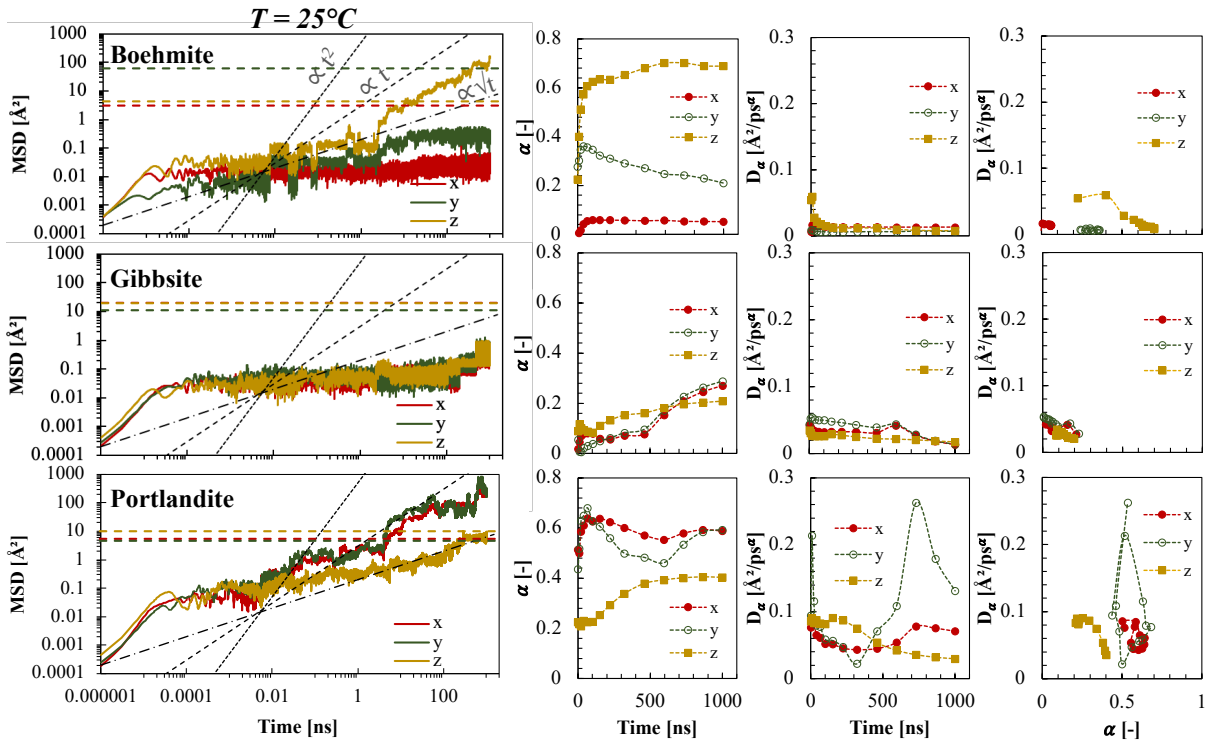

Figure 3: At left, mean squared displacement of H_2 in boehmite, gibbsite and portlandite at 25°C up to microsecond scale. The scaling with t^2 (ballistic, dotted line), t (Fickean, dashed line), and $\sqrt{t}$ (a specific case of strong subdiffusion, dot-dashed line) are shown for comparison. The horizontal lines corresponds to the squares of the distances between the endpoints of the NEB calculations with the same colour code as the MSD. At the center, α and D_α plotted as a function of the timescale considered. At the right, D_α as a function of α. The uncertainty in the values is on the order of 0.1 for α and 0.01 Å^2/ps$^\alpha$ for D_α.

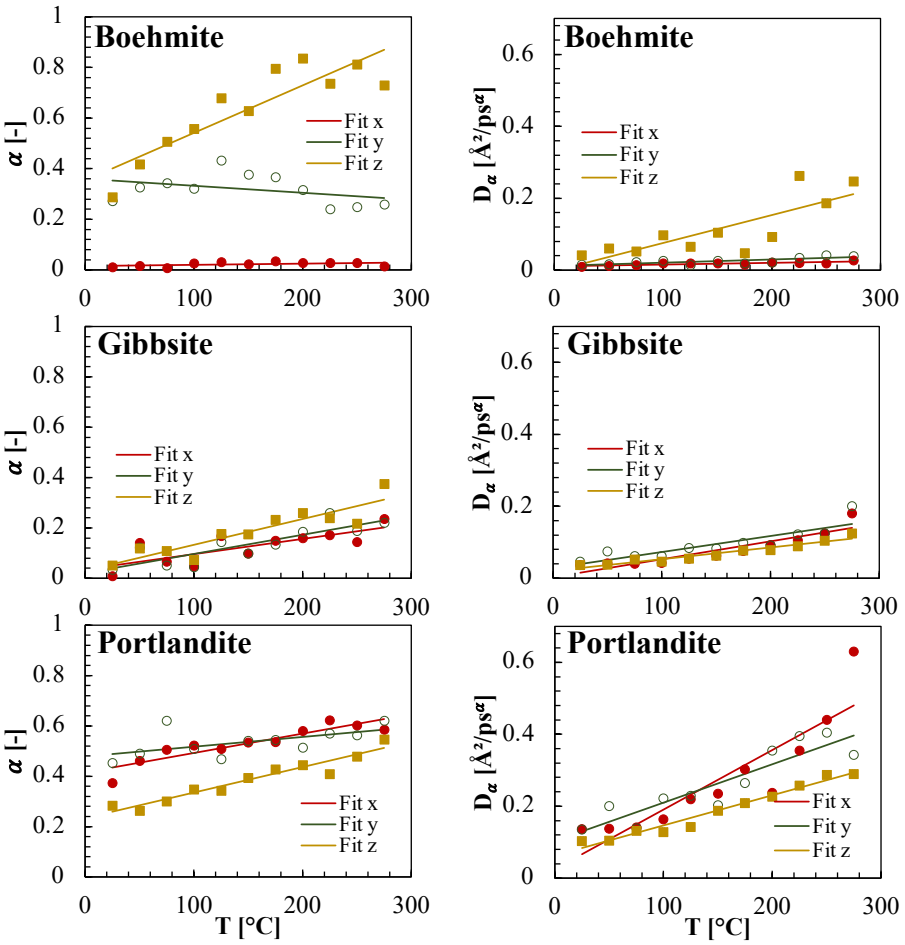

Figure 4: Anomalous exponent α (left) and generalized self-diffusion coefficient D_α (right) of H_2 in boehmite, gibbsite and portlandite as a function of the temperature. The linear fits are reported as guide for the eyes, the corresponding determination coefficients R_2 are listed in Table 2 together with the fitting parameters.

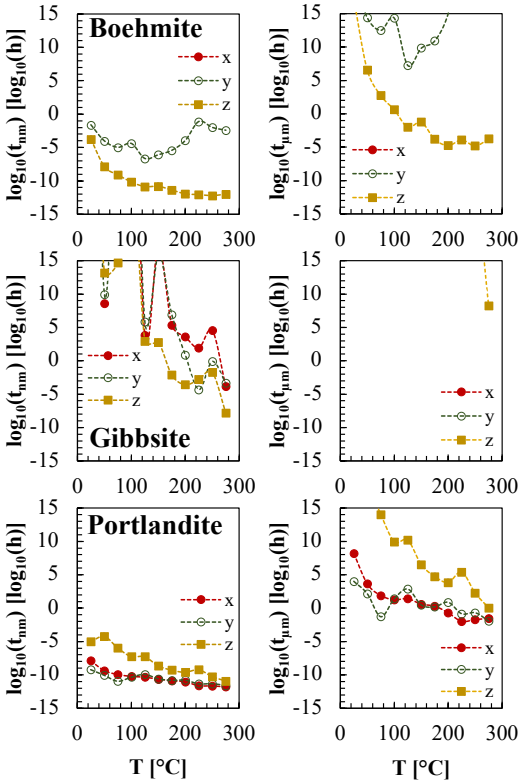

Figure 5: Quantification of H_2 mobility in boehmite, gibbsite and portlandite: characteristic time for mean displacement of one nanometer $t_{nm} = (1\ \mathrm{nm}^2/D_\alpha)^{(1/\alpha)}$ and one micrometer $t_{\mu m} = ((1000\ \mathrm{nm})^2/D_\alpha)^{(1/\alpha)}$. The results exceeding 10^{15} h (e.g., x direction in boehmite) are not shown since this is a timescale comparable to estimates of the universe's age.

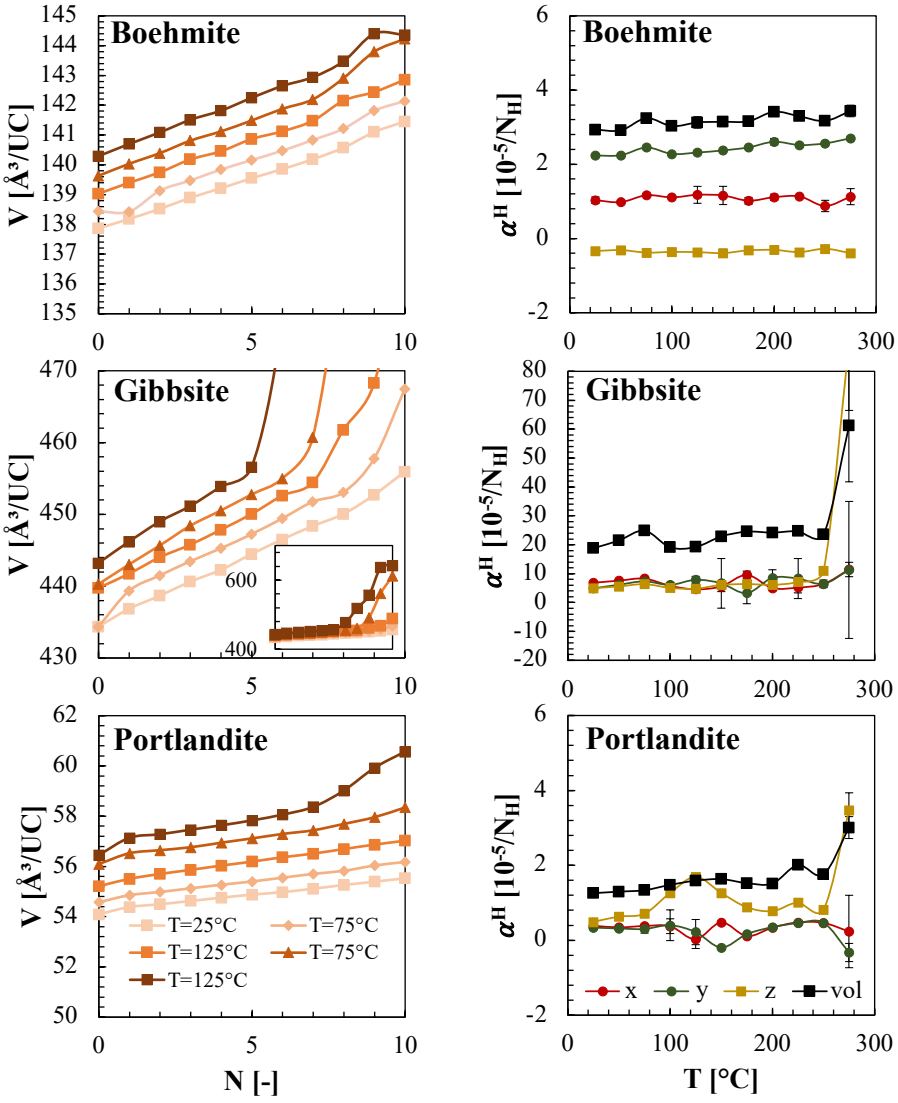

Figure 6: H_2-induced dilatation in boehmite, gibbsite, and portlandite. At left, volume per unit cell as a function of the number N of H_2 molecules introduced per simulation box. The inset shows the total expansion in gibbsite. At the right, linear (along cartesian direction x, y and z) and volumetric coefficients of H_2-induced dilatation α^H per number of H_2 molecules N_H per unit cell.

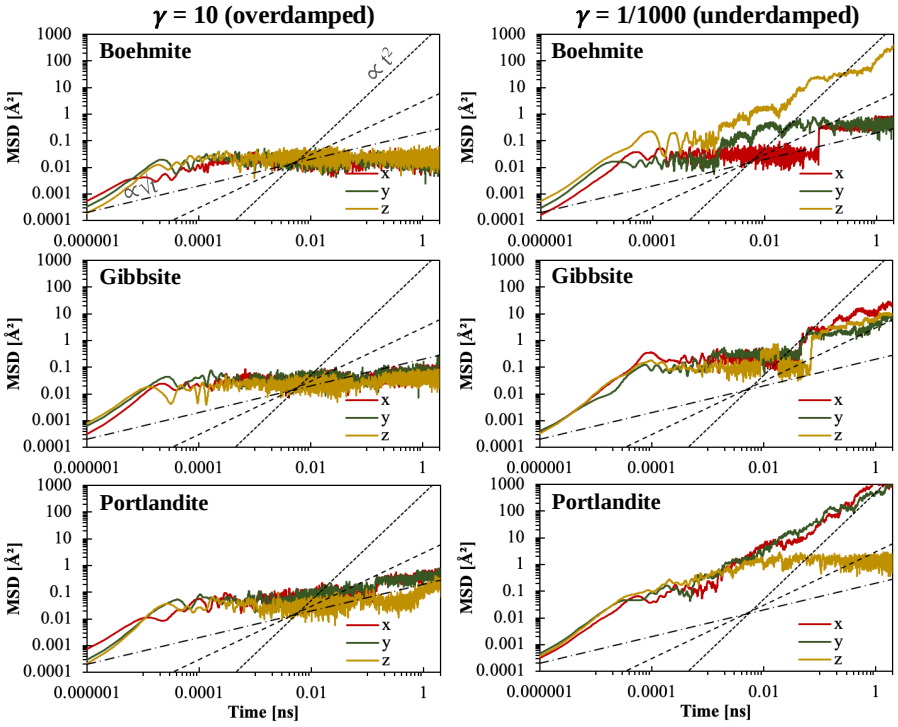

Figure 7: Mean squared displacement of H_2 in boehmite, gibbsite and portlandite at 25°C up to nanosecond scale considering damping parameters γ/ϵ_{HX} of 10 (left, overdamped leading to increased subdifusion) and 1/1000 (right, underdamped). The scaling with t^2 (ballistic, dotted line), t (Fickean, dashed line), and $\sqrt{t}$ (a specific case of strong subdiffusion, dot-dashed line) are shown for comparison.

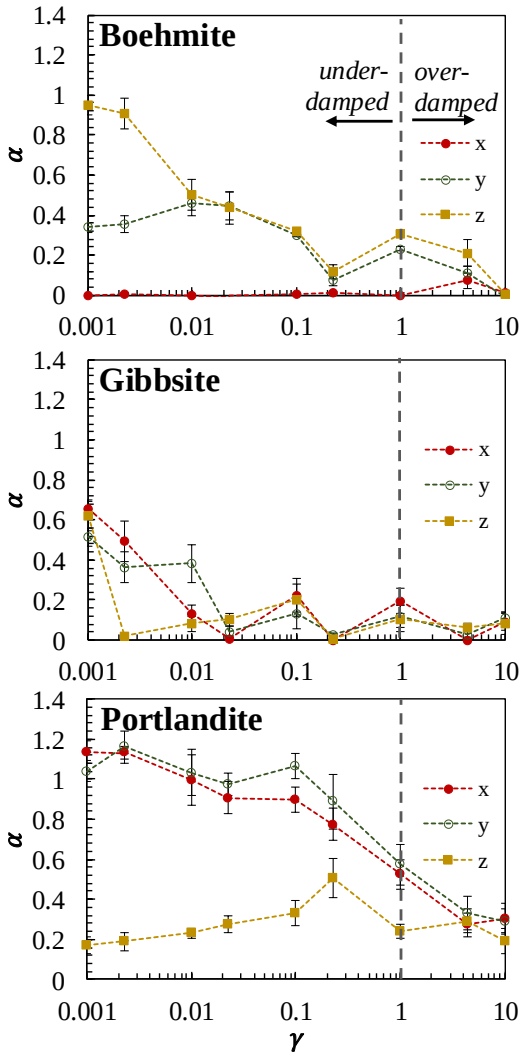

Figure 8: Anomalous exponent α as a function of affinity parameters γ/ϵ_{HX} in boehmite, gibbsite and portlandite simulated at 25°C.